ARTICLES

Journal of Semiconductors
(2019) 40, 122701
doi: 10.1088/1674-4926/40/12/122701

Simulation and application of external quantum efficiency of solar cells based on spectroscopy

Guanlin Chen[1, 2, 3], Can Han[1, 2, 3], Lingling Yan[1, 2, 3], Yuelong Li[1, 2, 3], Ying Zhao[1, 2, 3], and Xiaodan Zhang[1, 2, 3, †]

[1]Institute of Photoelectronic Thin Film Devices and Technology of Nankai University, Tianjin 300071, China

[2]Key Laboratory of Photoelectronic Thin Film Devices and Technology of Tianjin, Tianjin 300071, China

[3]Collaborative Innovation Center of Chemical Science and Engineering (Tianjin), Tianjin 300072, China

Abstract: In this study, a method for optical simulation of external quantum efficiency (EQE) spectra of solar cells based on spectroscopy is proposed, which is based on the tested transmittance and reflectance spectra. First, to obtain a more accurate information of refractive index and extinction coefficient values, we modified the reported optical constants from the measured reflectance and transmittance spectra. The obtained optical constants of each layer were then collected to simulate the EQE spectra of the device. This method provides a simple, accurate and versatile way to obtain the actual optical constants of different layers. The EQE simulation approach was applied to the flat and textured heterojunctions with intrinsic layers (HIT) solar cells, respectively, which showed a perfect matching between the calculation results and the experimental data. Furthermore, the specific optical losses in different devices were analyzed.

Key words: EQE simulation; optical constants; spectroscopy

Citation: G L Chen, C Han, L L Yan, Y L Li, Y Zhao, and X D Zhang, Simulation and application of external quantum efficiency of solar cells based on spectroscopy[J]. *J. Semicond.*, 2019, 40(12), 122701. http://doi.org/10.1088/1674-4926/40/12/122701

1. Introduction

Optical analysis from an EQE simulation features an explicit understanding of the current loss mechanisms within a PV device and gives practical guidelines for further device optimization[1, 2]. Among the various approaches that have been proposed, the optical admittance method[3] has provided a common basis for EQE simulations in a variety of applications, such as $CuIn_{1-x}Ga_xSe_2$[4], perovskite[5], and c-Si heterojunction[6]. This provides theoretical guidance for the design and optimization of high-efficiency solar cells.

A crucial step in the EQE simulation is to obtain the refractive index n and extinction coefficient k (are termed as the optical constants) of each layer of the solar cells. The methods that are commonly used to obtain such optical constants include spectroscopic ellipsometry (SE)[4, 5, 7, 8], heterodyne interferometry[9, 10], shift-coherent interferometry[11, 12], spectroscopy[13–17], etc. At present, SE is the most popular option because it can provide precise data of the tested materials, but also involves a complex process and a considerable equipment cost. Some commercial software packages, such as Scout[18] launched by WTheiss Hardware and Software Co. Ltd., can obtain the actual n and k values according to the measured transmittance and reflectance curves using appropriate fitting modes. However, they have matching problems and cost issues.

In this study, we have established a method that obtains the accurate optical constants of the tested layers simply by modifying the reported standard data based on the measured reflectance and transmittance curves, from which the obtained n, k values are treated as the actual data in device and then applied in the practical EQE simulation. This procedure enables the EQE of solar cells to be obtained in a simple, accurate, and computational cost-efficient way, which can provide a reliable optical analysis for devices fabricated in different specific experimental conditions. To further look into the feasibility of this method, we simulated the EQE of the flat and textured c-Si heterojunction with intrinsic layers (HIT) solar cells using several techniques and our calculation results have provided a remarkable agreement with the experimental data.

2. Experimental data

In this study, the EQE spectra of c-Si HIT solar cell[19] has been simulated and analyzed. Fig. 1 shows the structure of the solar cells, including Fig. 1(a) flat HIT solar cell and Fig. 1(b) textured HIT solar cell. The devices were fabricated on 275-μm thick, double-polished, (111) oriented, n-type float zone wafers, in which textured substrates were made from a hot potassium hydroxide solution. For the flat device fabrication process, 4-nm thick intrinsic a-Si:H (i-a-Si:H) and 20-nm thick n-type a-Si:H(n-a-Si:H) layers were first deposited via plasma-enhanced chemical vapor deposition (PECVD) on the rear side of silicon wafers at substrate temperature values of 130 and 180 °C, respectively. Then, 4-nm thick i-a-Si:H and 8-nm thick p-type a-Si:H (p-a-Si:H) layers were deposited on the front side of the wafers at substrate temperature values of 130 and 180 °C, respectively. Then, 90-nm thick ITO layers were deposited on the front side by thermal evaporation at 190 °C. Finally, the front silver (Ag) grid lines and rear aluminum (Al) electrodes were evaporated at room temperature. Meanwhile, to obtain the actual optical constants of the films in actual devices, each deposited film was prepared on the 1-

Correspondence to: X D Zhang, xdzhang@nankai.edu.cn
Received 1 APRIL 2019; Revised 18 MAY 2019.

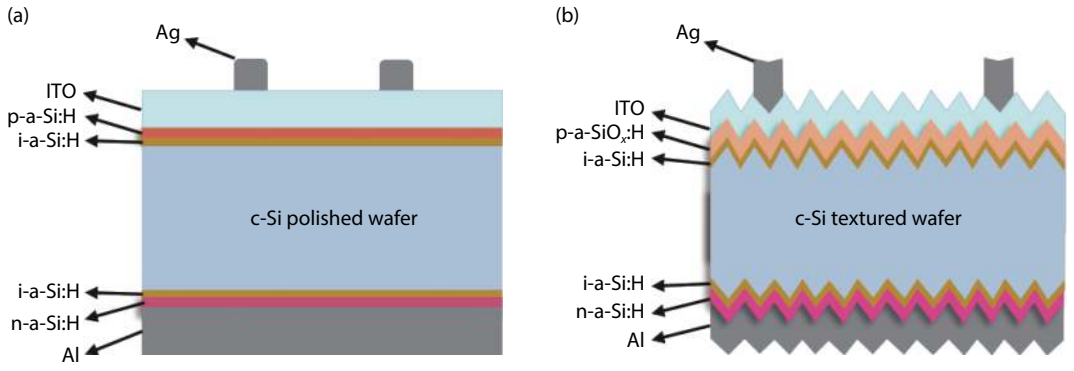

Fig. 1. (Color online) Structures of (a) flat and (b) textured HIT solar cell in this study.

mm thick glass by the same process used in device fabrication, after which corresponding transmittance and reflectance curves of each film was measured via UV–Vis–NIR system. Furthermore, to get an accurate evaluation of our calculation method, a p-type a-SiO_x:H (p-a-SiO_x:H) layer and a Ag/Al rear electrode layer were also deposited for the analysis among different optical performances. For the textured device process, all of the layers were the same with that of the flat device except the emitter layer, which was 8-nm p-a-SiO_x:H. The thickness of these films on the glass was measured by a step profiler. We assumed that the thickness of the film used in the device was approximately equal to the value obtained from the film deposited on the glass due to the same process. Transmittance and reflectance curves were measured by a UV–Vis–NIR system, and the bare glass is served the baseline to directly measure the transmittance and reflectance of the film for subsequent fitting.

3. Principle of EQE simulation

3.1. Optical constants obtained by spectroscopy

In this study, the optical constants of each film were obtained by simply measured transmittance and reflectance curves from UV–Vis–NIR spectroscopy. The procedure goes as follows: first, some sets of optical constants among expected wavelength range corresponding to different layers can be acquired from public resources[20–23], which will be the standard reference values and serve as initial data; second, the thickness, transmittance and reflectance curves of the deposited films will be measured by step profiler and UV–Vis–NIR system, respectively; and finally, the standard reference data is simply modified until the calculated transmittance and reflectance curves perfectly match the actual measured curves, the calculated curves can then be treated as the actual data of the deposited film, and the corresponding n, k values will serve as the real optical constants of the actual layer.

The modification process is related to the conclusion that n and k are wavelength-dependent functions, and every function of λ may be expressed by means of an infinite power series[20], followed by[21]:

$$n(\lambda) = a_{\mathrm{n}} + \frac{b_{\mathrm{n}}}{\lambda} + \frac{c_{\mathrm{n}}}{\lambda^2} + \cdots, \tag{1}$$

$$k(\lambda) = a_{\mathrm{k}} + \frac{b_{\mathrm{k}}}{\lambda} + \frac{c_{\mathrm{k}}}{\lambda^2} + \cdots. \tag{2}$$

Here, a_{n}, b_{n}, c_{n}, a_{k}, b_{k}, c_{k}… are constants.

According to Eqs. (1) and (2), the difference between the initial data $n(\lambda)$, $k(\lambda)$ and the modified data can be expressed by

$$\Delta n(\lambda) = \Delta a_{\mathrm{n}} + \frac{\Delta b_{\mathrm{n}}}{\lambda} + \frac{\Delta c_{\mathrm{n}}}{\lambda^2} + \cdots, \tag{3}$$

$$\Delta k(\lambda) = \Delta a_{\mathrm{k}} + \frac{\Delta b_{\mathrm{k}}}{\lambda} + \frac{\Delta c_{\mathrm{k}}}{\lambda^2} + \cdots, \tag{4}$$

where $\Delta n(\lambda)$ and $\Delta k(\lambda)$ represent the difference values and the actual optical constants can then be expressed as $n(\lambda)$ + $\Delta n(\lambda)$ and $k(\lambda)$ + $\Delta k(\lambda)$. The Δa_{n}, Δb_{n}, Δc_{n}, Δa_{k}, Δb_{k}, Δc_{k}… are the main parameters and the main work is to find these parameters in Eq. (3) and Eq. (4) to minimize the following functions:

$$\Delta F = \left(\sum_{\lambda} \left(R_{\mathrm{calculated}} - R_{\mathrm{measured}}\right)^2 + \left(T_{\mathrm{calculated}} - T_{\mathrm{measured}}\right)^2 \right)^{\frac{1}{2}}, \tag{5}$$

where R_{measured} and T_{measured} are the measured reflectance and transmittance in a proper wavelength range (such as 300–1200 nm), respectively, and the $R_{\mathrm{calculated}}$, $T_{\mathrm{calculated}}$ represent the corresponding calculated data. The numerical value of the ΔF can give us an estimation on the fit of reflectance and transmittance curves.

The method presented above is based on the Cauchy dispersion formula[22] and it may be applied for films from relatively transparent materials and with thicknesses greater than 0.2 mm[21]. However, we aim to demonstrate the possibilities of applying this method to other non-transparent materials because the reported optical constants of these materials already contained the original optical information.

We applied this method to ITO, p-a-Si:H, i-a-Si:H and n-a-Si:H based on the reported optical constants of these films[23, 24]. Fig. 2 shows the fitting results between the measured transmittance and reflectance curves and the calculated curves. To reduce the test error, the thickness of a-Si:H films on glass are thicker than that in the solar cell device. It should be noted that the optical constants will be similar since the thickness changes not so large[24, 25] (no more than 30 nm). As can be seen from the figures, the calculated curves showed a good agreement with the measured data of both reflectance and transmittance. The calculated optical con-

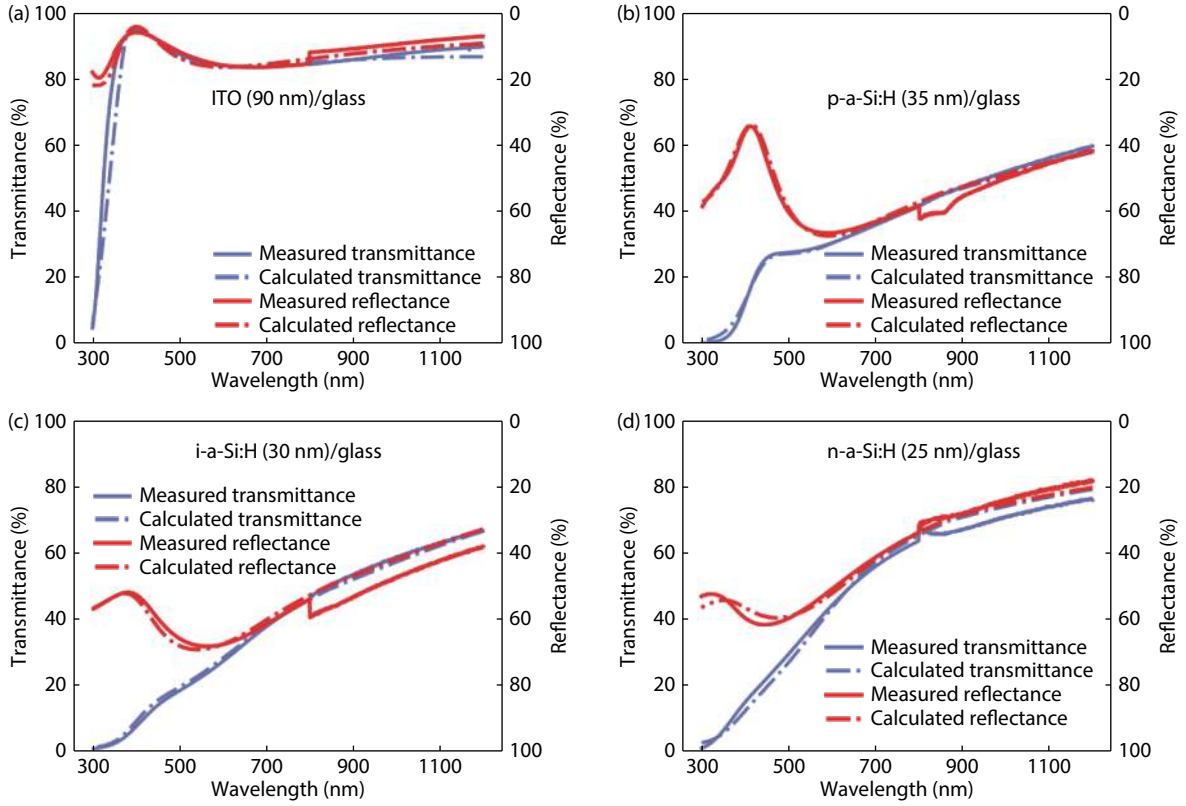

Fig. 2. (Color online) The fitting results of measured/calculated transmittance and reflectance curves of different layers. (a) ITO. (b) p-a-Si:H. (c) i-a-Si:H. (d) n-a-Si:H.

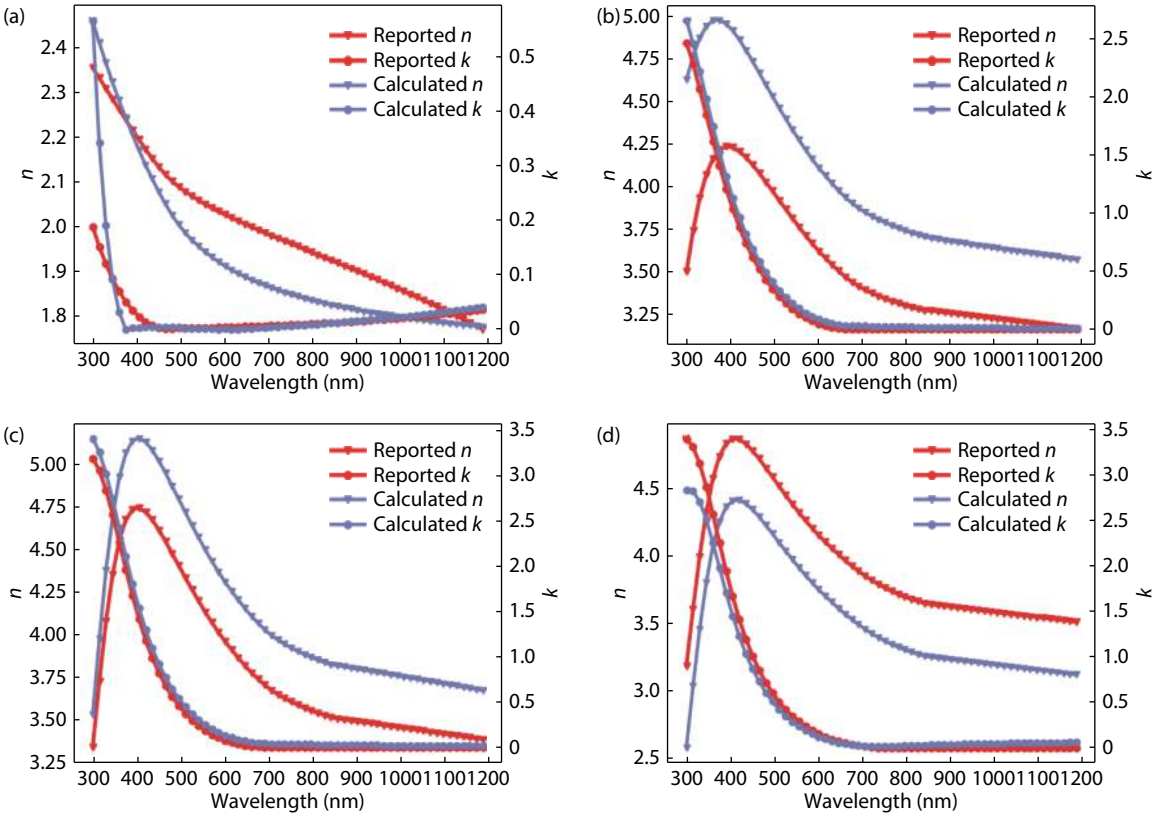

Fig. 3. (Color online) The calculated results of optical constants of different layers. (a) ITO. (b) p-a-Si:H. (c) i-a-Si:H. (d) n-a-Si:H.

stants of each layer are shown in Fig. 3. According to the figures, the calculated optical constants had the same trends compared with the reported optical constants, illustrating that the calculated optical constants had the same dispersion model as the reported optical constants. Therefore, by combining Fig. 2 and Fig. 3, we can see that the calculated results of optical constants were considered as the actual constants of these materials.

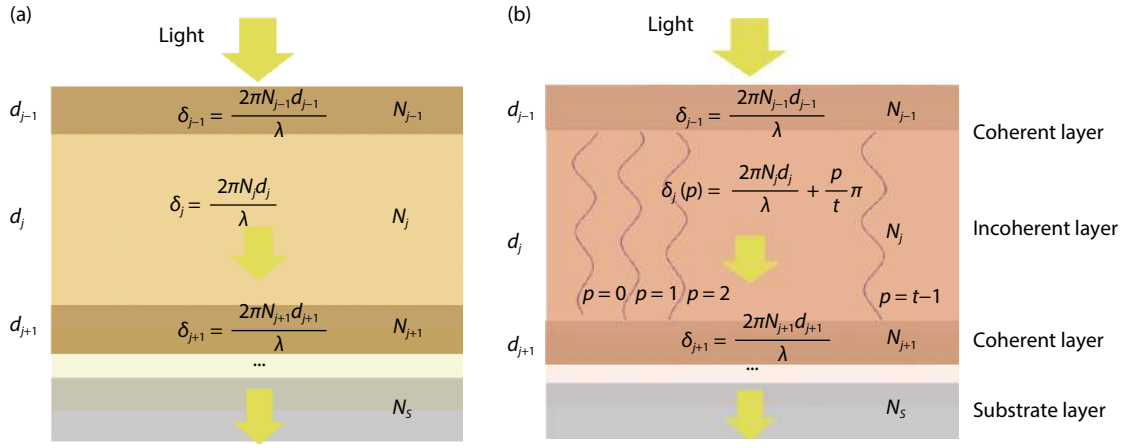

Fig. 4. (Color online) Schematic optical model of (a) multi-layer system with all coherent layers and (b) multi-layer system with coherent and incoherent layers.

The obtained n, k values of these materials will serve as the usable parameters in the following EQE calculation.

3.2. EQE calculation method

Most solar cells generally consist of transparent conductive oxide (TCO) layers, an active absorption layer and rear contact materials. From an optical point of view, this device can be considered as a multi-layer film system composed of absorption and non-absorption layers[26]. The optical admittance method has been applied to establish an optical model of this multi-layer film system for EQE calculation[4–6]. Fig. 4(a) shows the structure of this optical model. In this model, it is assumed that there are a total of m layers in the multi-layer film system, and the parameters of each film include thickness d_j and complex refractive index N_j (j = 1, 2, …, m), and the complex refractive index of the substrate N_s. The complex refractive index N can be expressed as $N = n - ik$, where n and k represents the refractive index and the extinction coefficient respectively. The optical admittance η is expressed as[27]

$$\eta = H/E, \tag{6}$$

where H and E are the magnetic and electric fields, respectively. The η can also be expressed as $\eta = NY$[3], where Y is unity, η and N are numerically the same. The transmittance and reflectance can be determined by solving the characteristic matrix of the multilayer film system, which is expressed by[27]

$$\begin{bmatrix} B \\ C \end{bmatrix} = \left\{ \prod_{j=1}^{m} \begin{bmatrix} \cos\delta_j & \frac{i}{\eta_j}\sin\delta_j \\ i\eta_j \sin\delta_j & \cos\delta_j \end{bmatrix} \right\} \begin{bmatrix} 1 \\ \eta_s \end{bmatrix}. \tag{7}$$

Here, η_j and η_s are the optical admittance of the jth layer and the substrate respectively. δ_j shows the phase thickness expressed as $\delta_j = 2\pi N_j d_j/\lambda$, here, d_j and λ are the thickness of the jth layer and wavelength, respectively.

The reflectance R can then be obtained by[27]

$$R = \frac{|n_0 - Y_{\text{eff}}|^2}{|n_0 + Y_{\text{eff}}|^2}, \tag{8}$$

where n_0 is the refractive index of air, which equals to 1. Y_{eff} is the effective optical admittance Y_{eff} of the multi-layer film system which can be expressed as $Y_{\text{eff}} = C/B$

The transmittance T can be obtained by

$$T = (1 - R)\frac{\text{Re}(N_s)}{\text{Re}(BC^*)}. \tag{9}$$

The absorptance A of the multi-layer film system can thus be written as $A = 1 - T - R$.

However, this method can only be employed under an coherent condition. For most solar cells, the optical response needs to be calculated under an incoherent condition. Fujiwara *et al.* have established an optical model in coherent and incoherent multi-layer film systems[6] (CPA method) by introducing the transfer matrix method into the optical admittance model. According to this model (seen from Fig. 4(b)), the δ_j should be expressed by[6]

$$\delta_j(p) = \frac{2\pi N_j d_j}{\lambda} + \frac{p}{t}\pi, \tag{10}$$

where t is the total number of assumed waves and p is the serial number of each wave (p = 0, 1, 2, …, t – 1). Then the reflectance R_{CPA} in this method can be expressed by[6]

$$R_{\text{CPA}} = \frac{1}{t}\sum_{p=0}^{t-1} \frac{|n_0 - Y_{\text{eff}}(\delta_j(p))|^2}{|n_0 + Y_{\text{eff}}(\delta_j(p))|^2}. \tag{11}$$

Here, the $Y_{\text{eff}}(\delta_j(p))$ represents optical admittance of the overall multi-layer system in which the pth wave in the coherent layer were concerned.

The transmittance T_{CPA} can be obtained using Eq. (8)

$$T_{\text{CPA}} = (1 - R_{\text{CPA}})\frac{1}{t}\sum_{p=0}^{t-1} \frac{\text{Re}(N_s)}{\text{Re}(BC^*(\delta_j(p)))}, \tag{12}$$

where the $BC^*(\delta_j(p))$ represents the calculated BC^* of the overall multi-layer system in which the pth wave in the coherent layer were concerned, which is shown in Fig. 4(b).

Finally, the absorptance can be determined as follows[6]

$$A = (1 - R_{\text{CPA}})\left(1 - \frac{1}{t}\sum_{p=0}^{t-1} \frac{\text{Re}(N_s)}{\text{Re}(BC^*(\delta_j(p)))}\right). \tag{13}$$

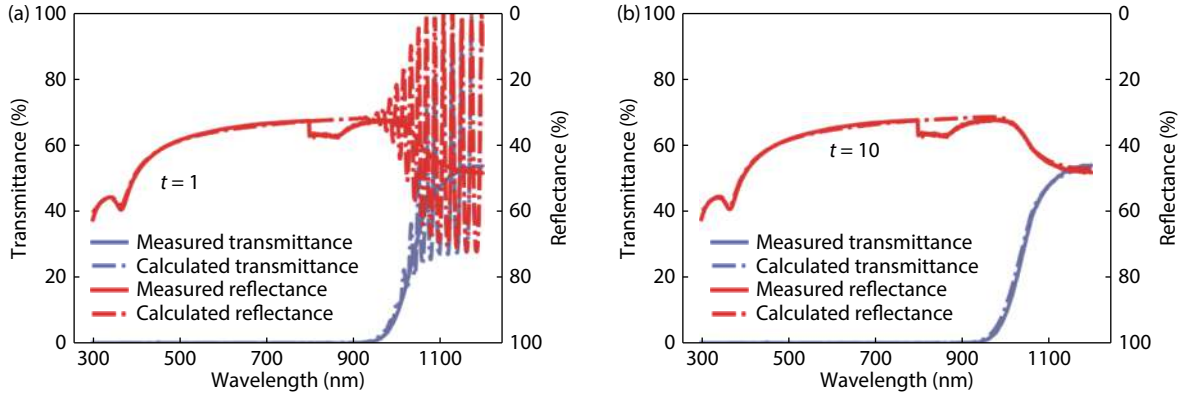

Fig. 5. (Color online) The fitting results of measured/calculated transmittance and reflectance curves on a modified c-Si thickness of 8000 nm with (a) $t = 1$ in Eq. (10), and (b) $t = 10$ in Eq. (10).

Based on this method, the total absorptance of the flat solar cell can be calculated. When the carrier collection rate is 100%, EQE = A. However, in the actual process, due to the parasitic absorption, carriers cannot be completely collected. Therefore, for a flat solar cell containing an absorbing layer and other functional layers, the EQE can be obtained by[28]

$$\mathrm{EQE} = 1 - R - A_{\mathrm{p}}^{\mathrm{front}} - A_{\mathrm{p}}^{\mathrm{back}}, \tag{14}$$

where $A_{\mathrm{p}}^{\mathrm{front}}$ and $A_{\mathrm{p}}^{\mathrm{back}}$ represent the parasitic absorption of the front and the back layers of the solar cell which can be obtained based on the above optical model, respectively. Since most rear electrodes of the solar cell allow no transmission, such as silver or aluminum, the total A of the device can be expressed as $A = 1 - R$[29], which includes $A_{\mathrm{p}}^{\mathrm{front}}$, $A_{\mathrm{p}}^{\mathrm{back}}$ and the absorptance of the active layer, and the absorptance of the active layer is the EQE of the solar cell device.

For textured solar cells, Eq. (11) cannot be used because the reflectance is significantly lower in visible light region than that of flat solar cell[30], which is due to the antireflection effect of the textured surface, thus the reflectance of the textured solar cell needs to be measured. The actual reflectance of a textured solar cell can be measured as R_{EPS}, the total absorptance of the textured solar cell A_{tex} can then be expressed by[30]

$$A_{\mathrm{tex}} = (1 - R_{\mathrm{EPS}})\left(1 - \frac{1}{t}\sum_{p=0}^{t-1}\frac{\mathrm{Re}(N_s)}{\mathrm{Re}(BC^*(\delta_{\mathrm{j}}(p)))}\right). \tag{15}$$

Using the same method as the flat device, the EQE of textured solar cell can also be calculated.

4. Results

4.1. Simulation and analysis of flat HIT solar cell

The actual optical constants of each layer of the flat HIT solar cell were obtained by the above method. For the case of the bulk c-Si, air was used as the substrate. Unfortunately, since 275-μm thick c-Si is not comparable with other layers in thickness value, the result of Y_{eff} will become very large, which is quite difficult to calculate. Therefore, the thickness of c-Si used for calculation must also be decreased to a range that can be calculated by the computer. However, decreasing the thickness will inevitably reduce the absorption of c-Si[31]. Therefore, in this study, the absorption coefficient α is increased while decreasing the thickness of c-Si to ensure the consistence between the calculated absorptance and the actual absorptance of c-Si. Because the α of c-Si in the short wavelength region is greater than that in the long wavelength region[32], combined with the Beer-Lambert's law ($I(x) = I_0\exp(-\alpha x)$), all of the short-wavelength light can be absorbed within a short distance from the front surface of the c-Si; however, the long-wavelength light requires a longer distance to be absorbed[33]. Consequently, in this study the thickness of c-Si is decreased to 8000 nm and the k values were increased only in the long wavelength region to increase the $\alpha(k = \alpha\lambda/4\pi)$ to match the actual absorptance of c-Si. Fig. 5 shows the fitting results of c-Si with a manipulated thickness of 8000 nm. Fig. 5(a) shows the fitting results with $t = 1$ in Eq. (10), where a quite sharp optical interference can be seen in the long wavelength region (> 1000 nm). Fig. 5(b) corresponds to the results with $t = 10$ in Eq. (10), in which the optical interference was visibly eliminated and quite smooth curves which matched well with the experimental data were obtained, indicating that the 8000 nm c-Si could perform the same optical properties with the original 275-μm c-Si and ensure an effective foundation for subsequent calculation. As for the Al film, the optical constants were obtained by fitting the measured transmittance and reflectance curves of Al/Glass through iterative calculation based on the reported data[34].

By applying the modified optical constants of these films into Eq. (7), the characteristic matrix of the device can be obtained, and finally the EQE can be calculated from Eq. (14). Fig. 6(a) shows the comparison between the calculated EQE and the measured EQE of the flat HIT solar cell. It can be seen again that with $t = 1$ in Eq. (10), the optical interference occurred in the long wavelength region, which would be eliminated in the case of $t = 10$ in Eq. (10), thus resulted in a remarkable matching between the calculated curves and the experimental data. The integrated current of the cell from the EQE spectra was 35.2 mA/cm^2 (measured) and 34.3 mA/cm^2 (calculated), respectively. This difference was attributed to the optical response in the short wavelength region, which can be explained by the difference between the thickness of the films measured on glass and the thickness of each layer in the actual device in the calculation process. Figs. 6(b) and 6(c) show EQE spectra with different p-a-Si:H and i-a-Si:H thicknesses, from which we can see that with the thickness of p-a-Si:H or a-Si:H increasing, the EQE data showed distinctly different

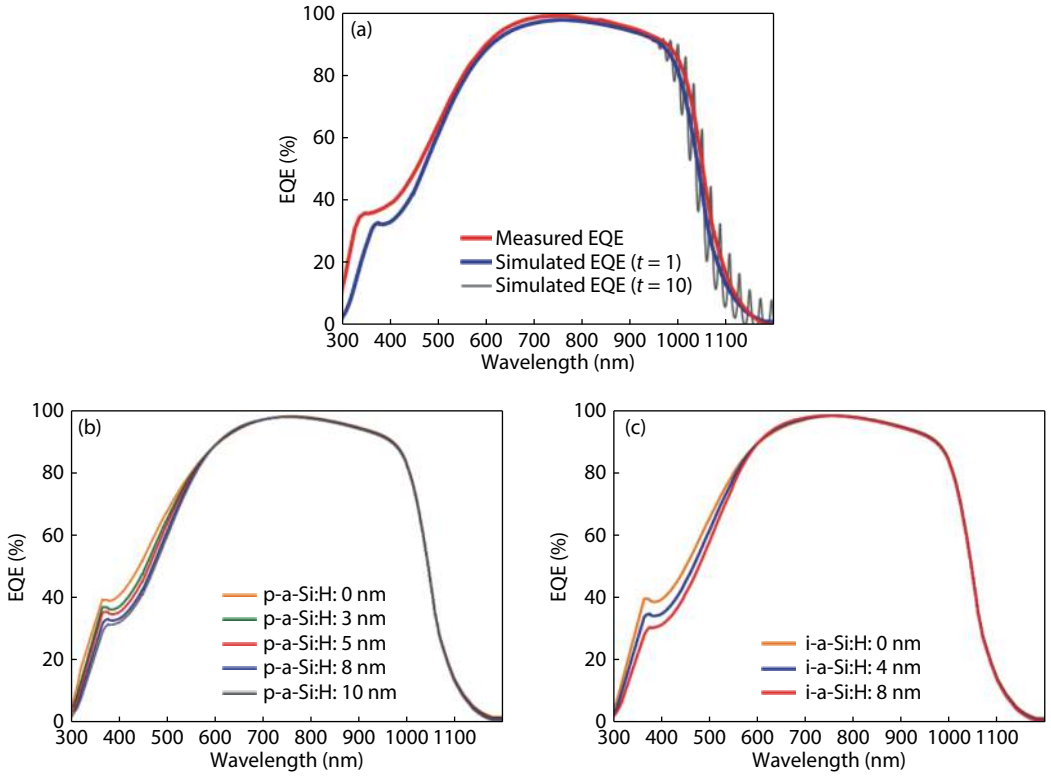

Fig. 6. (Color online) The calculation results of EQE simulation on the flat HIT solar cells. (a) The fitting results between the measured EQE and different calculated curves. (b) and (c) The EQE sensitivity on the thickness of p-a-Si:H and i-a-Si:H layers, respectively.

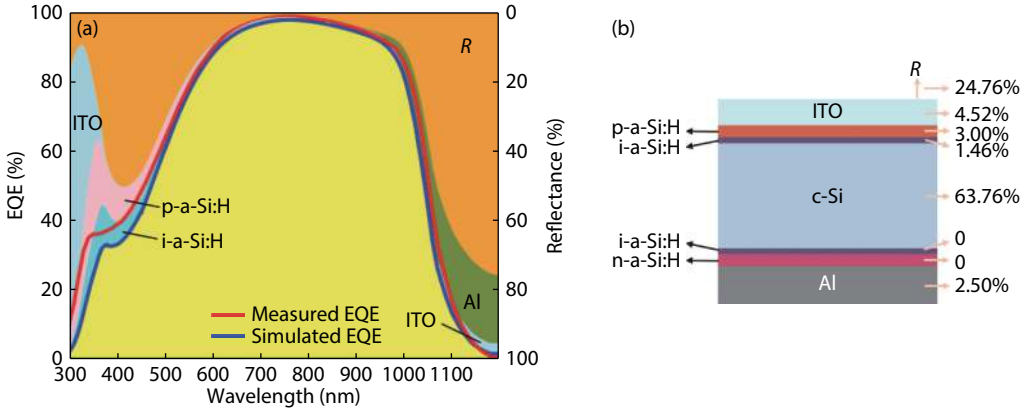

Fig. 7. (Color online) Optical analysis of the flat HIT solar cell. (a) Measured/calculated EQE results. (b) The contribution of each layer on the current loss (or gain) in the device.

curves in the short wavelength region[23]. The results show that the optical response in short wavelength were very sensitive to the thickness of a-Si layers, either in the doping p-a-Si:H layer or intrinsic i-a-Si:H layer. This phenomenon provided some accessorial proof to explain the mismatching in the short wavelength of Fig. 6(a). Furthermore, the thickness difference in the a-Si layers did not change the optical response in the visible and infrared wavelength range, indicating no observable parasitic absorption of a-Si:H layers in these wavelength ranges.

Based on an integral process, the optical contribution of each layer of the flat HIT solar cell was further calculated, as shown in Fig. 7. Furthermore, Fig. 7(a) gives an EQE analysis on the device, with different color region corresponding to different optical loss (or gain) of each component layer, while Fig. 7(b) represents a clear numerical summary of the mentioned current contributions. In the short wavelength region, the parasitic absorption of ITO and a-Si:H layers have taken up most of the total absorption, which is an important limiting factor on the short-circuit current density J_{sc} of the HIT solar cells since the carrier collection here is almost 0[24]. As for the long wavelength region (> 1000 nm), our results show that the parasitic absorption of metal electrode (Al) was significant, whereas the parasitic absorption from the ITO layer was negligible in this simulation.

4.2. EQE calculation of HIT with p-a-SiO$_x$:H

To increase the current from short wavelength, an emitter layer of p-a-SiO$_x$:H has been utilized to substitute p-a-Si:H, due to its wider optical band gap[35–37]. Figs. 8(a) and 8(b) show the results corresponding to the flat HIT solar cell

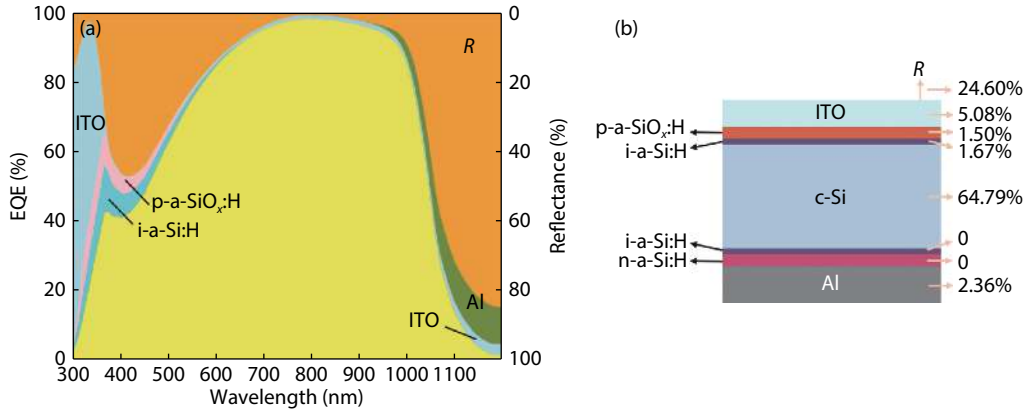

Fig. 8. (Color online) Calculation results of flat HIT solar cell with p-a-SiO_x:H as the front doping layer. (a) EQE calculation results. (b) The contribution of each layer on the current loss (or gain) in the device.

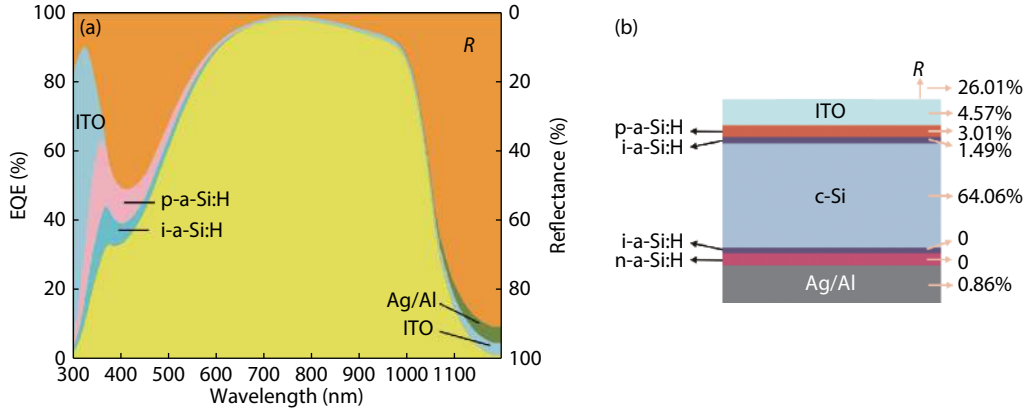

Fig. 9. (Color online) Calculation results of flat HIT solar cell with Ag/Al electrode as rear metal layer. (a) EQE calculation results. (b) The contribution of each layer on the current loss (or gain) in the device.

with p-a-SiO_x:H as the doping layer, accordingly. We can see that the current loss from p-a-SiO_x:H was 1.50%, which is much less than the value of 3.00% from the case of utilizing p-a-Si:H as the doping layer. That is to say, we could expect a reduction of almost 50% in the parasitic absorption of p-a-Si:H by replacing it with p-a-SiO_x:H. It is noteworthy that the overall current gains from such a replacement was about 0.2 mA/cm^2, which was consistent with the reported results[37, 38]. These data give us a clear understanding of the expected performance from doped p-a-SiO_x:H layers, and also indicates the accuracy and feasibility of our calculation method.

4.3. EQE calculation of HIT with Ag/Al electrode as rear metal layer

To further evaluate the current improvement in the long wavelength region (> 1000 nm), we utilized Ag/Al to replace Al as the rear metal layer in HIT solar cells[39]. Figs. 9(a) and 9(b) demonstrate the calculation results with such a design, from which we can see that with Ag/Al electrode, the rear metal layer only contributed 0.86% to the current loss in the device EQE, which was much less than the value of 2.50% in Fig. 7(b), indicating a significant reduction of the parasitic absorption of metal. The reason for this lies in the high back reflectance of Ag/Al electrode[35, 39–41], evidence of which could be also found in the increased contribution percentage of both c-Si and the overall reflectance. To summarize, we can expect another reduction of > 60% in the parasitic absorption of Al by replacing it with Ag/Al electrode, and the overall current improvement was about 0.2 mA/cm^2 in our experimental condition.

4.4. EQE simulation and analysis of textured HIT solar cell

This simulation method for the flat HIT solar cell can also be applied to the textured HIT solar cells. The difference is that the reflectance of the textured solar cell has to be actually measured since the anti-reflection effect of the textured c-Si is difficult to calculate. Based on the R_{EPS}, the EQE of the textured HIT solar cell can be calculated from Eq. (15), corresponding optical loss (gains) could be analyzed in the same way as the case in the flat HIT solar cells. It should also be noted that the top angle of pyramid-shaped texture is confirmed to be 80°[42, 43] and the calculated refractive index of ITO, p-a-Si:H, i-a-Si:H and c-Si are 1.93, 3.58, 3.65 and 3.54, which results in transmission angles of Air/ITO, ITO/p-a-Si:H and p-a-Si:H/i-a-Si:H, i-a-Si:H/c-Si of 24°, 13°, 13° and 13°, respectively. Consequently, in the calculation process of textured solar cell, a normal incidence of light is assumed because the transmission angles are close to the normal to the {111} texture-facet plane[6].

Fig. 10(a) shows the calculated result for a textured HIT solar cell. Again, the calculated curve shows a perfectly matching with the measured data, and the integrated current of the cell from the EQE spectra was 39.2 mA/cm^2 (measured) and 39.1 mA/cm^2 (calculated), respectively. Fig. 10(b) corresponds to the calculated contribution of each layer on the cur-

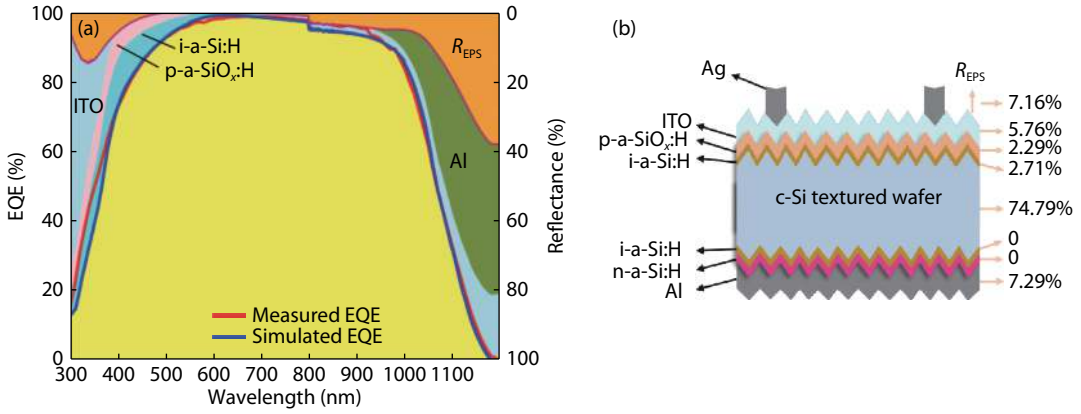

Fig. 10. (Color online) Optical analysis of the textured HIT solar cell. (a) Measured/calculated EQE calculation results. (b) The contribution of each layer on the current loss (or gain) in the device.

rent loss (or gain) in the device. Compared with the calculated results of the flat solar cell in Fig. 8(b), the overall reflection of the device was decreased by ~70%, accompanied by a preferable increase of ~20% in the absorption of the bulk c-Si, as well as an unavoidable increase in the parasitic absorption of the rear Al layer due to more light trapping in the device.

5. Conclusion

We established a spectroscopy-based method to obtain the actual optical constants of the layers in a solar cell device for the optical simulation of EQE. Combined with the measured transmittance and reflectance spectra from UV–Vis–NIR system and some sets of public standard reference data, a modification on optical constants was conducted via simple computational calculation, from which corresponding *n*, *k* values can be obtained and served as the actual data in the device. This approach enables us to develop an accurate EQE simulation method. The calculation results show remarkable agreements with the experimental data, both in flat and textured HIT applications. Furthermore, different contributions of each layer on the overall current loss (or gain) have been analyzed. In addition, different promising techniques related to the considerations in different wavelength ranges have been applied to our calculation method. The results show that a doped p-a-SiO_x:H layer in the front side can repress ~50% of the parasitic absorption of p-a-Si:H in the short wavelength, while we can expect another reduction of > 60% of the parasitic absorption of Al electrode in the long wavelength region by utilizing Ag/Al as rear metal layers. These routines indicate the practical accuracy and versatility of our EQE simulation approach. Finally, an ongoing study of our calculation method in other photovoltaic devices has been made and will be reported in the future.

Acknowledgement

The authors gratefully acknowledge the supports from National Key Research and Development Program of China (Grant No. 2018YFB1500103), National Natural Science Foundation of China (Grant Nos. 61474065 and 61674084), Tianjin Research Key Program of Science and Technology (Grant No. 18ZXJMTG00220), 111 Project (Grant No. B16027), and Fundamental Research Funds for the Central Universities.

References

[1] Ding K, Kirchartz T, Pieters B E, et al. Characterization and simulation of a-Si:H/μc-Si:H tandem solar cells. Sol Energy Mater Sol Cells, 2011, 95(12), 3318

[2] Jošt M, Köhnen E, Morales-Vilches A B, et al. Textured interfaces in monolithic perovskite/silicon tandem solar cells: advanced light management for improved efficiency and energy yield. Energy Environ Sci, 2018, 11(12), 3511

[3] Macleod H A. Thin-film optical filters. New York: Taylor and Francis Ltd, 2001

[4] Hara T, Maekawa T, Minoura S, et al. Quantitative assessment of optical gain and loss in submicron-textured $CuIn_{1-x}G\ a_xSe_2$ solar cells fabricated by three-stage coevaporation. Phys Rev Appl, 2014, 2(3), 034012

[5] Nakane A, Tampo H, Tamakoshi M, et al. Quantitative determination of optical and recombination losses in thin-film photovoltaic devices based on external quantum efficiency analysis. J Appl Phys, 2016, 120(6), 064505

[6] Nakane A, Fujimoto S, Fujiwara H. Fast determination of the current loss mechanisms in textured crystalline Si-based solar cells. J Appl Phys, 2017, 122(20), 203101

[7] Aspnes D E, Studna A. A high precision scanning ellipsometer. Appl Opt, 1975, 14(1), 220

[8] Jakopic G, Papousek W. Unified analytical inversion of reflectometric and ellipsometric data of absorbing media. Appl Opt, 2000, 39(16), 2727

[9] Chiu M H, Lee J Y, Su D C. Complex refractive-index measurement based on Fresnel's equations and the uses of heterodyne interferometry. Appl Opt, 1999, 38(19), 4047

[10] Chiu M H, Lee J Y, Su D C. Refractive-index measurement based on the effects of total internal reflection and the uses of heterodyne interferometry. Appl Opt, 1997, 36(13), 2936

[11] Cheng Y Y, Wyant J C. Multiple-wavelength phase-shifting interferometry. Appl Opt, 1985, 24(6), 804

[12] Cheng Y Y, Wyant J C. Two-wavelength phase shifting interferometry. Appl Opt, 1984, 23(24), 4539

[13] Leveque G, Villachon-Renard Y. Determination of optical constants of thin film from reflectance spectra. Appl Opt, 1990, 29(22), 3207

[14] Siqueiros J M, Regalado L E, Machorro R. Determination of (*n, k*) for absorbing thin films using reflectance measurements. Appl Opt, 1988, 27(20), 4260

[15] Al-Kuhaili M F, Khawaja E E, Durrani S M. Determination of the optical constants (*n* and *k*) of inhomogeneous thin films with linear index profiles. Appl Opt, 2006, 45(19), 4591

[16] Cisneros J I. Optical characterization of dielectric and semiconductor thin films by use of transmission data. Appl Opt, 1998,

37(22), 5262
[17] Katsidis C C, Siapkas D I. General transfer-matrix method for optical multilayer systems with coherent, partially coherent, and incoherent interference. Appl Opt, 2002, 41(19), 3978
[18] http://www.wtheiss.com/
[19] Taguchi M, Yano A, Tohoda S, et al. 24.7% record efficiency HIT solar cell on thin silicon wafer. IEEE J Photovolt, 2014, 4(1), 96
[20] Stroud K A. Engineering mathematics. New York: Springer-Verlag, 1992
[21] Nenkov M, Pencheva T. Calculation of thin-film optical constants by transmittance-spectra fitting. J Opt Soc Am A, 1998, 15(7), 1852
[22] Likhachev D A. Practical method for optical dispersion model selection and parameters variations in scatterometry analysis with variable *n*&*k*'s. Thin Solid Films, 2014, 562, 90
[23] Holman Z C, Filipič M, Descoeudres A, et al. Infrared light management in high-efficiency silicon heterojunction and rear-passivated solar cells. J Appl Phys, 2013, 113(1), 013107
[24] Holman Z C, Descoeudres A, Barraud L, et al. Current losses at the front of silicon heterojunction solar cells. IEEE J Photovolt, 2012, 2(1), 7
[25] Chambouleyron I, Ventura S, Birgin E, et al. Optical constants and thickness determination of very thin amorphous semiconductor films. J Appl Phys, 2002, 92(6), 3093
[26] Zhu F, Singh J. Study of the optical properties of amorphous silicon solar cells using admittance analysis. J Non-Cryst Solids, 1993, 152(1), 75
[27] Lin C W, Chen K P, Su M C, et al. Admittance loci design method for multilayer surface plasmon resonance devices. Sens Actuators B, 2006, 117(1), 219
[28] Theuring M, Geissendörfer S, Vehse M, et al. Thin metal layer as transparent electrode in n–i–p amorphous silicon solar cells. EPJ Photovolt, 2014, 5(55205), 55205
[29] Margulis G Y, Hardin B E, Ding I K, et al. Parasitic absorption and internal quantum efficiency measurements of solid-state dye sensitized solar cells. Adv Energy Mater, 2013, 3(7), 959
[30] Zhang D, Digdaya I A, Santbergen R, et al. Design and fabrication of a SiO_x/ITO double-layer anti-reflective coating for heterojunction silicon solar cells. Sol Energy Mater Sol Cells, 2013, 117(14), 132
[31] Ghica C, Nistor L C, Teodorescu V S, et al. Laser treatment of plasma-hydrogenated silicon wafers for thin layer exfoliation. J Appl Phys, 2011, 109(6), 063518
[32] Wang H, Liu X, Zhang Z M. Absorption coefficients of crystalline silicon at wavelengths from 500 nm to 1000 nm. Int J Thermophys, 2013, 34(2), 213
[33] Davis K, Seigneur H, Jiang K, et al. Optical modeling of the internal back reflectance of various c-Si dielectric stacks featuring AlO_x, SiN_x, TiO_2 and SiO_2. 38th IEEE Photovoltaic Specialists Conference (PVSC), 2012: 1032
[34] McPeak K M, Jayanti S V, Kress S J, et al. Plasmonic films can easily be better: rules and recipes. ACS Photonics, 2015, 2(3), 326
[35] Seif J P, Descoeudres A, Filipič M, et al. Amorphous silicon oxide window layers for high-efficiency silicon heterojunction solar cells. J Appl Phys, 2014, 115(2), 024502
[36] Sritharathikhun J, Yamamoto H, Miyajima S, et al. Optimization of amorphous silicon oxide buffer layer for high-efficiency p-type hydrogenated microcrystalline silicon oxide/n-type crystalline silicon heterojunction solar cells. J Appl Phys, 2008, 47(11R), 8452
[37] Fujiwara H, Kaneko T, Kondo M. Application of hydrogenated amorphous silicon oxide layers to c-Si heterojunction solar cells. Appl Phys Lett, 2007, 91(13), 133508
[38] Battaglia C, De Nicolas S M, De Wolf S, et al. Silicon heterojunction solar cell with passivated hole selective MoO_x contact. Appl Phys Lett, 2014, 104(11), 113902
[39] Zhang X, Zhao Y, Gao Y, et al. Influence of front electrode and back reflector electrode on the performances of microcrystalline silicon solar cells. J Non-Cryst Solids, 2006, 352(9–20), 1863
[40] Holman Z C, Descoeudres A, Wolf S D, et al. Record infrared internal quantum efficiency in silicon heterojunction solar cells with dielectric/metal rear reflectors. IEEE J Photovolt, 2013, 3(4), 1243
[41] Silva K S B D, Keast V J, Gentle A, et al. Optical properties and oxidation of α-phase Ag–Al thin films. Nanotechnology, 2017, 28(9), 095202
[42] Matsuki N, Fujiwara H. Nondestructive characterization of textured a-Si:H/c-Si heterojunction solar cell structures with nanometer-scale a-Si:H and In_2O_3:Sn layers by spectroscopic ellipsometry. J Appl Phys, 2013, 114(4), 18
[43] Watanabe K, Matsuki N, Fujiwara H. Ellipsometry Characterization of hydrogenated amorphous silicon layers formed on textured crystalline silicon substrates. Appl Phys Express, 2010, 3(11), 116604